Optics Letters

On-chip single-mode high-Q terahertz whispering gallery mode resonator

Ziwei Wang,[1] Shixing Yuan,[1] Gaoneng Dong,[1] Ruolan Wang,[1] Liao Chen,[1,4] Xiaojun Wu,[2,3] and Xinliang Zhang[1]

[1]Wuhan National Laboratory for Optoelectronics and School of Optical and Electronic Information, Huazhong University of Science and Technology, Wuhan 430074, China
[2]School of Electronic and Information Engineering, Beihang University, Beijing 100191, China
[3]e-mail: xiaojunwu@buaa.edu.cn
[4]e-mail: liaochenchina@hust.edu.cn

Received 12 March 2019; revised 1 May 2019; accepted 8 May 2019; posted 8 May 2019 (Doc. ID 362239); published 28 May 2019

The chip-scale terahertz (THz) devices and systems are helpful to enable actual applications in THz communication and sensing. Here, we demonstrate an on-chip THz whispering gallery mode resonator (WGMR) delivering a high-quality (Q) factor TE single mode, fabricated on a high-resistivity float zone silicon wafer by complementary metal–oxide–semiconductor compatible technology. For a TE mode in a WGMR, it is the first time to achieve a Q factor of 1210 at 0.4925 THz with 28 dB extinction ratio, to the best of our knowledge. With this excellent WGMR, we have demonstrated a stable and highly sensitive sensor for particle distance estimation. Our investigation provides an effective approach to fabricate high-performance integrated THz-WGMRs for chip-scale systems. © 2019 Optical Society of America

https://doi.org/10.1364/OL.44.002835

High-performance integrated terahertz (THz) devices with low-cost, efficient, scalable, and configurable characteristics are highly demanded, especially in the practical applications of THz wireless communications [1] and highly sensitive sensing [2,3]. Compared with plenty of THz resonators having the virtue of a high-quality (Q) factor and sensitivity to demonstrating versatile functional devices based on metamaterials [4], photonic crystals [5], and metal waveguides [6], whispering gallery mode resonators (WGMRs) feature their unique properties such as possessing unprecedented high-Q factors [7,8]. As we know, WGMRs in the optical domain [9] are attracting more and more attention because of their broad application fields from fundamental physics to promising signal processing. Compared with that in the optical domain, researches on THz-WGMRs have just started. Recently, a quartz bubble resonator with a Q factor of 440 was successfully demonstrated at 0.45 THz in 2018 [7]. When the material was changed to high-resistivity float zone silicon (HRFZ-Si), and the shape was fabricated to a sphere, the Q factor was dramatically increased to 15,000 [8], which demonstrates that HRFZ-Si is one of the most promising materials for realizing THz-WGMRs with low absorption loss. However, these THz-WGMRs are all separated devices and work independently, which suffer from less scalability and poor stability. On-chip WMGRs based on HRFZ-Si holds numerous merits of high stability, small size, low cost, and compatibility of the complementary metal–oxide–semiconductor (CMOS) process, which may have great potential for applications in filters, delay lines, sensors, and beyond [10–12]. Recently, one on-chip THz-WGMR device was demonstrated successfully based on HRFZ-Si [13]. It exhibits good performances with a Q factor of 2839 for the $TM_{0,0}$ mode at 218 GHz and a Q factor of 168 for the $TE_{0,0}$ mode at 189 GHz. Considering the integration of various function devices on one chip, the tailor of TM modes always relies on varying the heights to satisfy the needs of the required functions, which usually needs tedious processes of multiple overlay. On the contrary, the tailor of TE modes usually depends on different widths, and it can be easily realized just by designing the masks. Therefore, devices based on TE modes are more mutually compatible and more flexible. Moreover, the single-mode WGMR has the advantage of high spectral purity and small mode volume area [14]. Therefore, it is significant to demonstrate a high-Q factor for TE single mode on a chip.

In this work, we demonstrate a TE single-mode high-Q THz-WGMR fabricated on HRFZ-Si wafer with conventional CMOS technology. By optimizing the parameters of the WGMR, we obtain a Q factor of 1210 for the TE single mode with 28 dB extinction ratio (ER). Then, we qualitatively corroborate its high sensitivity for this TE mode by varying the effective refractive index (n_{eff}) through changing the distance between the quartz particle and the ring resonator surface. Using this THz-WGMR, we can experimentally monitor the variation of the effective refractive index.

In the THz frequency range of <1 THz, HRFZ-Si holds the advantages of very low loss (<0.025 cm^{-1}) and high refractive index ($n = 3.416$) [15], and it is well compatible with the CMOS technology. Therefore, we choose to fabricate the integrated THz-WGMRs on HRFZ-Si with a resistivity of more than 10 $\mathrm{k\Omega \cdot cm}$. The schematic diagram of the designed THz-WGMR for ~0.5 THz is illustrated in Fig. 1(a). It includes a straight coupling waveguide and a ring resonator etched on a

double-side polished HRFZ-Si wafer. We set the gap between the ring resonator and the waveguide as g and the radius of the ring as r. In addition, in the detailed figure of the waveguide cross-section, the thickness of the wafer and the height of the ridge are set as H and h, respectively, and the width of the ridge is set as w. The cross-section dimensions of the ring resonator and the coupling waveguide are consistent. To realize the high-Q TE single mode, we use commercial COMSOL software to optimize the cross-section of the ridge waveguide [16].

In order to comply with the TE single-mode condition and avoid the emergence of TM mode for high spectral purity and small mode volume area, the cross-section parameters (H, h, w) of the ridge waveguide should be well designed. Firstly, w stays at 500 μm, while H and h are varied to avoid the existence of the TM mode, as shown in Fig. 1(b). As an example, when H and h are set as 200 μm and 100 μm, respectively, the waveguide still supports the existence of the $TM_{0,0}$ mode, as illustrated in Fig. 1(b)(i). When H is reduced to 120 μm ($h = 60$ μm), the waveguide cannot excite the TM mode, as shown in Fig. 1(b)(ii). Thus, we choose $H = 120$ μm and $h = 60$ μm. Then, w is designed to satisfy the TE single-mode condition. As shown in Fig. 1(c)(i)–1(c)(ii), if the width of the ridge is too narrow ($w = 200$ μm), there is no $TE_{1,0}$ mode. But, the electric field of the $TE_{0,0}$ mode has strong interaction with the sidewall of the ridge, which will lead to a high scattering loss due to the sidewall roughness in fabrication. On the contrary, if the width of the ridge is too wide ($w = 400$ μm), the waveguide will also support the $TE_{1,0}$ mode, as illustrated in Fig. 1(c)(v)–1(c)(vi). When the width of the ridge is set as 300 μm, only a fundamental $TE_{0,0}$ mode can be supported, as shown in Fig. 1(c)(iii)–1(c)(iv). Therefore, we set the waveguide cross-section parameters H, h, and w as 120, 60, and 300 μm, respectively, in order to realize the single TE mode and high-Q THz-WGMRs.

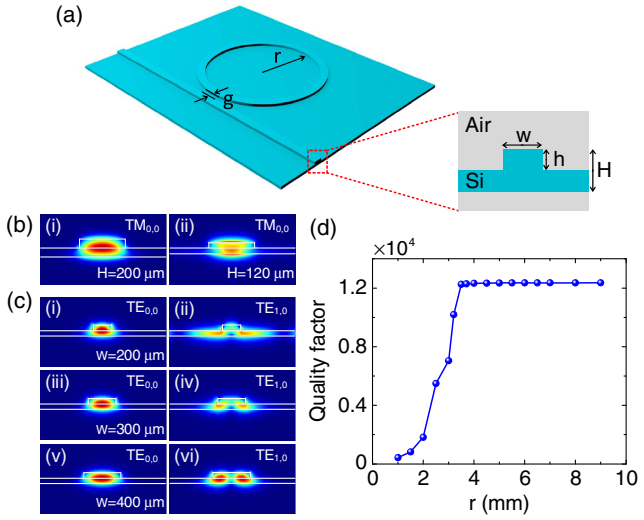

Fig. 1. Schematic diagram and design of the THz-WGM resonator. (a) Schematic diagram of the THz-WGM resonator where the inserted figure on the right is the cross-section of the ridge waveguide. (b) The simulated electric-field (E) distribution of $TM_{0,0}$ modes with different thickness of wafer H. H is (i) 200 and (ii) 120 μm, respectively. The height of the ridge h is half of H, while the width of the ridge w is always 500 μm. The polarizations of $TM_{0,0}$ modes are both vertical to the plate. (c) The simulated electric-field (E) distribution of the $TE_{0,0}$ mode (left) and $TE_{1,0}$ mode (right) with different w. w is (i)–(ii) 200 μm, (iii)–(iv) 300 μm, and (v)–(vi) 400 μm, respectively. The polarizations of two modes are both parallel to the plate. H and h are always 120 and 60 μm, respectively. (d) The calculated intrinsic Q factor as a function of the ring radius. H, h, and w are 120, 60, and 300 μm, respectively.

The intrinsic Q factors as a function of the ring radius r are calculated, as shown in Fig. 1(d) [16]. It is mainly determined by the bending loss and HRFZ-Si absorption loss in the simulation. The intrinsic Q factor increases monotonously as the radius increases from 1 to 3.5 mm, which is attributed to the decreasing bending loss. When the radius is further increased, the intrinsic Q factor tends to a constant of 12,000, which is the theoretical limit. The ultimate limit is determined by the absorption loss of HRFZ-Si. To simultaneously achieve a high-Q factor and enable the size to be as small as possible, here we set the radius of the ring as 4 mm. In addition, the gap between the ring and the waveguide g is set to be 10 μm to guarantee the over-coupling state.

The THz-WGMRs are fabricated by using ultra-violet lithography (MJB 4) and inductively coupled plasma (ICP) (Oxford Plasmalab system 100 ICP180) deep etching. The coupling region between the ring resonator and the waveguide is characterized by an optical microscope. As illustrated in Fig. 2(a), the ridge width w of the fabricated waveguide is 279.7 μm, which is 20.3 μm less than the designed value, while the gap g is 32.1 μm, which is 22.1 μm larger than the designed value. These deviations are mainly caused by the ICP etch process. It is noted that this is a fixed deviation, which can be pre-compensated during the device design process. The cross-section of the ridge waveguide is also characterized by a scanning electron microscope (SEM). As illustrated in Fig. 2(b), the measured H and h are 126.75 and 60.78 μm, respectively, which agrees well with the designed value. In order to guarantee the TE single-mode condition, we use the measured parameters to simulate the electric-field distribution of the ridge waveguide again, and it still works well. On the other hand, besides the absorption loss of the material, the scattering loss caused by the sidewall roughness also influences the Q factor. Therefore, it is essential to make the sidewall as smooth as possible. Figure 2(b) indicates that the fabricated sidewall is relatively smooth, which is very helpful to achieve a high-Q factor.

The fabricated THz-WGMR is measured by THz vector network analyzers (VNA) (Ceyear 3649B) delivering a frequency range from 0.325 to 0.5 THz, and the metal waveguide internal dimension of the emitter is 508 × 254 μm^2 (WR-2.2). The schematic diagram of the experimental setup is shown in Fig. 3(a). A linearly polarized THz wave is generated from the emitter, then horizontally coupled into the silicon waveguide,

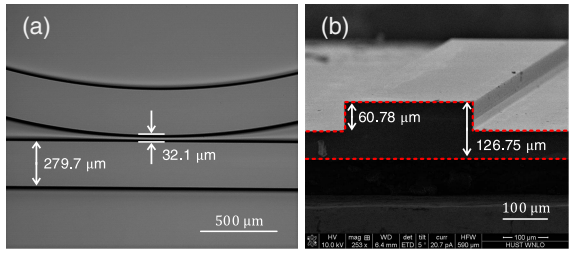

Fig. 2. Fabricated THz-WGM resonator. (a) An optical microscopic image of the coupling area. (b) A SEM image of the ridge waveguide cross-section.

and excites a TE mode. Then, the THz wave propagates along the waveguide and couples into the ring resonator. Finally, the THz wave is probed by the receiver of VNA. As the THz frequency is swept in the VNA, the intensity and phase transmission spectra can both be acquired during the experiment. Figure 3(b) depicts the measured intensity and phase transmission spectra covering a frequency range from 0.46 to 0.5 THz. The frequency interval between adjacent resonances is uniform in the intensity transmission spectrum, which indicates that the device only supports a TE single mode. The resonance free spectral rang (FSR) of the WGMR is ∼2.4 GHz. Furthermore, it can be found that the ER is different at different resonant frequencies, which originates from multiple Fabry–Perot (FP) effects and the frequency dependent coupling coefficient [9]. From the phase response of the device, we can see that the WGMR is in the over-coupling state with the resonances from 0.46 to 0.5 THz. To characterize the Q factor of this device further, we choose a specific resonant frequency of 0.49246 THz and fit the experimental results with the transmission matrix method [8], as shown in Fig. 3(c). The amplitude transmissivity T_t and phase transmissivity Φ [17] can be expressed as

$$T_t = \frac{r^2 + a^2 - 2ar\cos\varphi}{1 + a^2r^2 - 2ar\cos\varphi}, \tag{1}$$

$$\Phi = \pi + \varphi + \tan^{-1}\frac{r\sin\varphi}{a - r\cos\varphi} + \tan^{-1}\frac{ar\sin\varphi}{1 - ar\cos\varphi}, \tag{2}$$

respectively, where a is the single-pass transmission coefficient of the ring, r is the coupling coefficient between the waveguide and the ring, $\varphi = \beta L$ represents the phase shift for one round-trip, L is the round-trip length, and β is the propagation constant. According to the fitting process, it is found that the full width at half-maximum (FWHM) of the resonance is 407 MHz, corresponding to a Q factor of 1210 at the frequency of 0.49246 THz. Moreover, the ER is as high as 27.7 dB. To the best of our knowledge, this is the highest measured Q factor for a TE single mode in on-chip THz-WGMRs.

WGMRs have great potential in the sensing field with the advantages of high-Q factor and evanescent field in the optical domain [18]. Recently, in the THz domain, WGMRs are also demonstrated to have excellent performances for sensing [12,19]. However, both of the previous works are based on discrete devices, including the separated coupling waveguide and sphere WGMRs. Here, we use the fabricated high-Q single-mode WGMR based on HRFZ-Si to implement a typical application experiment for sensing to verify its abilities. The schematic diagram of the sensing principle is shown in Fig. 4(a). A dielectric particle is located above the surface of the ring with a gap. The distance between the particle and the ring surface can

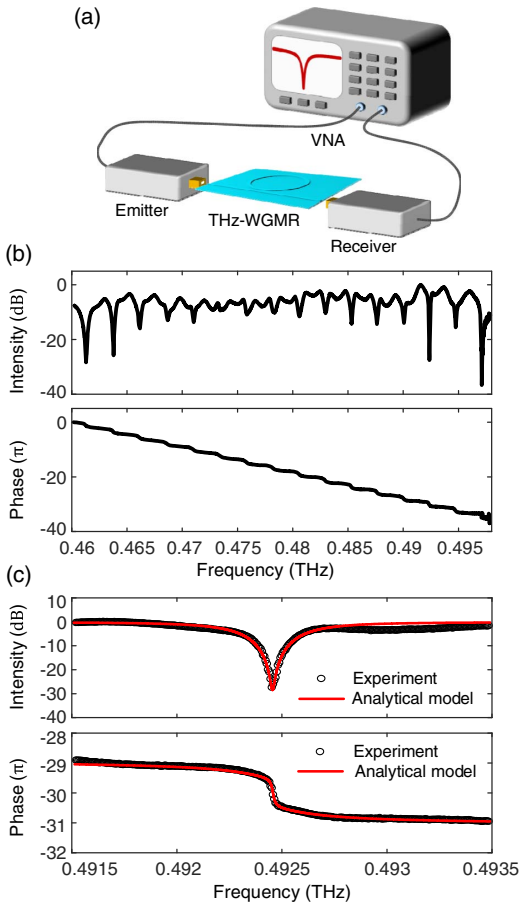

Fig. 3. Experimental setup and measured transmission results. (a) Illustration of the experimental setup. (b) The measured transmission intensity (upper) and phase profile (under) of the THz-WGMR in the over-coupling state with the frequency range of 0.46–0.5 THz. (c) The enlarged transmission intensity (upper) and corresponding phase profile (under) with the frequency around 0.4925 THz. The black circles represent experimental results, while the red line represents simulated results.

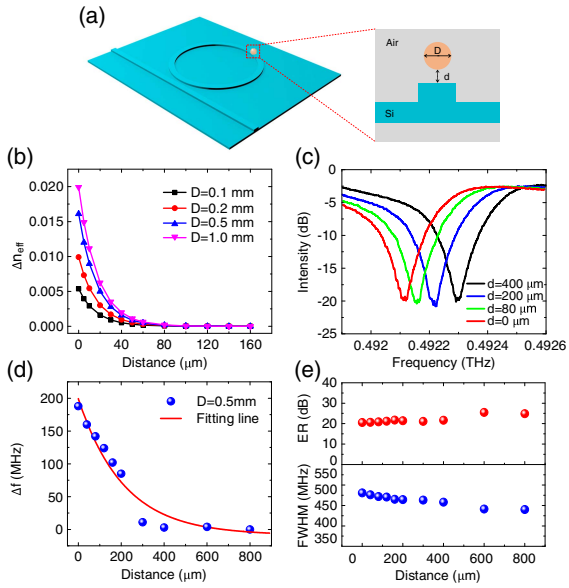

Fig. 4. Application of the THz-WGM resonator in sensing. (a) Schematic diagram of the sensing principle. D is the diameter of the quartz dielectric particle. d represents the distance between the particle and the surface of the ring. (b) The simulated results for the change of effective refractive index Δn_{eff} as a function of d with 0.1, 0.2, 0.5, and 1.0 mm particle diameter. (c) The measured transmission intensity spectra with different d. (d) The measured frequency redshift Δf as a function of d. The blue dots and red line represent the experimental results and the fitting line, respectively. (e) The ER (upper) and FWHM (under) of the measured transmission intensity spectra as a function of d.

be easily measured according to the frequency shift of the WGMR resonance. The particle is made of quartz, which has a refractive index of 1.96 and a relatively low material loss of about 0.2 cm^{-1} from 0.4 to 0.5 THz [20]. The diameter of the dielectric particle is defined as D, while the distance between the particle and the ring surface is defined as d. Before performing the sensing experiment, we have used commercial COMSOL software to simulate the effective refractive index perturbation Δn_{eff} caused by the dielectric particle with different D or d. The simulated results are shown in Fig. 4(b). The Ds are chosen as 0.1, 0.2, 0.5, and 1.0 mm, respectively. We can see that for a dielectric particle with a certain D, when the particle is far away from the ring surface, there is nearly no change in the n_{eff}. When the d is smaller than some fixed value (∼100 μm), the Δn_{eff} gradually increases with the decreased d. This is because when the d is small enough, the particle will interact with the evanescent field of the THz in the WGMR, resulting in an increase in the n_{eff} of the mode. It is also shown that the n_{eff} increases much faster for larger particles with a fixed d, which means that larger particles induce more serious interaction. The effective index perturbation of the WGMR will result in the frequency shift of the WGMR resonant frequency. Therefore, we can use the frequency shift of the resonance to measure the distance of a specific particle to the ring surface or the particle size for a fixed distance.

Taking the experimental conditions of our laboratory into consideration, we only have an optical fiber tip with a diameter of 0.5 mm available to verify the simulations on particle distance sensing. This experiment also uses the VNA to measure the frequency shift of the ring amplitude response, and the experimental setup is the same with that in Fig. 3(a). In addition, d is measured by the micrometer of a three-dimensional alignment jig, and the distance measurement accuracy is ∼5 μm. Figure 4(c) shows the transmission intensity responses of four different d. During the change of d, the spectra are clear to be distinguished because of the WGMR with the single mode and high Q. The resonant frequency shifts of all transmission responses are shown in Fig. 4(d). The red shift of the resonant frequency is observed as the particle gets closer to the WGMR, and the maximum frequency shift is 190 MHz. However, when d is larger than some fixed value (∼400 μm), there is no detectable resonance peak drift, which is accorded with the simulation results. Because of the limitation of our laboratory condition, the experimental and simulation models are slightly different, which results in the slight difference between the experimental and simulated distances. On the other hand, from the transmission intensity responses shown in Fig. 4(c), we can also see that the ER and the FWHM of the transmission spectra are stable during the sensing process. Figure 4(e) shows the detailed changes of ER and FWHM at different d. It is observed that the ER remains about 21 dB, and the deviation is less than 5 dB. The FWHM of the resonance decreases with the increase of d, and the bandwidth fluctuation is within 40 MHz. In the sensing experiment, the ER and FWHM both vary slightly, which shows the stability of the on-chip WGMR. Therefore, the integrated high-Q single-mode THz WGMR has been applied successfully as a stable and highly sensitive sensor for the distance between a particle and the ring surface. To the best of our knowledge, it is the first time the integrated WGMR sensor is shown in the THz domain.

In summary, an integrated TE single-mode THz-WGMR is proposed and experimentally demonstrated. The measured Q factor is as high as 1210 at the resonant frequency of 0.4925 THz, and the corresponding ER is 27.7 dB. With this on-chip high-Q single-mode device, we demonstrate a stable and highly sensitive sensor for particle distance estimation. This result shows that the on-chip THz-WGMR has great potential to be applied to specific cell detections and microfluid sensing. Moreover, this kind of on-chip THz device exhibits advantages of CMOS compatibility, high-Q factor, compactness, low cost, and large-scale integration, which can push forward the on-chip THz photonics as well as their practical applications.

Funding. National Natural Science Foundation of China (NSFC) (61735006); Laboratory Research Fund from Wuhan National Laboratory for Optoelectronics (2018WNLOKF001); China Postdoctoral Science Foundation (2018M640692); "Qingba" Program of Beihang University (KG12089701).

Acknowledgment. We thank the 41st Research Institute of China Electronics Technology Group Corporation (CETC) for providing the test equipment and the Center of Micro-Fabrication and Characterization (CMFC) of WNLO for providing the fabrication services.

REFERENCES

1. J. Ma, R. Shrestha, J. Adelberg, C. Y. Yeh, Z. Hossain, E. Knightly, J. M. Jornet, and D. M. Mittleman, Nature **563**, 89 (2018).
2. H. Tao, A. C. Strikwerda, M. Liu, J. P. Mondia, E. Ekmekci, K. Fan, D. L. Kaplan, W. J. Padilla, X. Zhang, R. D. Averitt, and F. G. Omenetto, Appl. Phys. Lett. **97**, 261909 (2010).
3. J. F. O'Hara, R. Singh, I. Brener, E. Smirnova, J. Han, A. J. Taylor, and W. Zhang, Opt. Express **16**, 1786 (2008).
4. M. Manjappa, P. Pitchappa, N. Singh, N. Wang, N. I. Zheludev, C. Lee, and R. Singh, Nat. Commun. **9**, 4056 (2018).
5. C. M. Yee and M. S. Sherwin, Appl. Phys. Lett. **94**, 154104 (2009).
6. V. Astley, B. McCracken, R. Mendis, and D. M. Mittleman, Opt. Lett. **36**, 1452 (2011).
7. D. W. Vogt and R. Leonhardt, Optica **4**, 809 (2017).
8. D. W. Vogt and R. Leonhardt, APL Photon. **3**, 051702 (2018).
9. W. Bogaerts, P. De Heyn, T. Van Vaerenbergh, K. De Vos, S. Kumar Selvaraja, T. Claes, P. Dumon, P. Bienstman, D. Van Thourhout, and R. Baets, Laser Photon. Rev. **6**, 47 (2012).
10. R. Mendis, A. Nag, F. Chen, and D. M. Mittleman, Appl. Phys. Lett. **97**, 131106 (2010).
11. S. Chauhan and R. Letizia, "Photonic crystal-microring resonators for tunable delay lines," arXiv:1811.07828 (2018).
12. C. Mathai, R. Jain, V. G. Achanta, S. P. Duttagupta, D. Ghindani, N. R. Joshi, R. Pinto, and S. S. Prabhu, Opt. Lett. **43**, 5383 (2018).
13. J. Xie, X. Zhu, X. Zang, Q. Cheng, L. Chen, and Y. Zhu, Opt. Mater. Express **8**, 50 (2018).
14. Y. A. Vlasov and S. J. McNab, Opt. Express **12**, 1622 (2004).
15. J. Dai, J. Zhang, W. Zhang, and D. Grischkowsky, J. Opt. Soc. Am. B **21**, 1379 (2004).
16. M. Oxborrow, IEEE Trans. Microwave Theory Tech. **55**, 1209 (2007).
17. D. G. Rabus, in *Integrated Ring Resonators* (2007), Vol. **127**, pp. 3–40.
18. J. Ward and O. Benson, Laser Photon. Rev. **5**, 553 (2011).
19. D. W. Vogt, A. H. Jones, H. G. L. Schwefel, and R. Leonhardt, "Anomalous blue-shift of terahertz whispering-gallery modes via dielectric and metallic tuning," arXiv:1901.03424 (2019).
20. S. Tsuzuki, N. Kuzuu, H. Horikoshi, K. Saito, K. Yamamoto, and M. Tani, Appl. Phys. Express **8**, 072402 (2015).

210.28.142.31 on 2024-04-13 08:14:37